Dalton Transactions

Accepted Manuscript

ROYAL SOCIETY OF CHEMISTRY

www.rsc.org/dalton

Journal Name

RSCPublishing

ARTICLE

The Influence of $NaYF_4$:Yb,Er Size/Phase on the Multimodality of Co-encapsulated Magnetic Photon-Upconverting Polymeric Nanoparticles

Cite this: DOI: 10.1039/x0xx00000x

Received 00th January 2014,
Accepted 00th January 2014

DOI: 10.1039/x0xx00000x

www.rsc.org/

Michael Challenor[1,2], Peijun Gong[3], Dirk Lorenser[3], Michael J. House[4], Robert C. Woodward[4], Timothy St. Pierre[4], Melinda Fitzgerald[2], Sarah A. Dunlop[2], David D. Sampson[3,5], K. Swaminathan Iyer[1*]

We report the synthesis, characterisation and evaluation of the *in vitro* biocompatibility of polymeric nanoparticles with both magnetic and upconverting fluorescent properties. The particles consist of superparamagnetic iron oxide nanoparticles and upconverting $NaYF_4$:Yb,Er nanoparticles co-encapsulated within a poly(glycidyl methacrylate) sphere. Two different upconverting nanoparticles (10 nm α-$NaYF_4$:Yb,Er and 50 nm β-$NaYF_4$:Yb,Er) were synthesised and the optical and magnetic properties of the composite polymeric nanoparticle systems assessed by near infra-red laser spectroscopy, SQUID magnetometry and proton relaxometry. A live-dead assay was used to assess the viability of PC-12 neural cells incubated with varying concentrations of the nanoparticles. The composite nanoparticles produced no observed impact on cellular viability even at concentrations as high as 1000 μg/mL. Confocal microscopy revealed uptake of nanoparticles by PC-12 cells and peri-nuclear cytoplasmic localisation. Both particle systems show favourable magnetic properties. However, only the nanospheres containing 50 nm β-$NaYF_4$:Yb,Er were suitable for optical tracking because the presence of iron oxide within the composites imparts a significant quenching of the upconversion emission. This study demonstrates the size and phase of the upconverting nanoparticles are important parameters that have to be taken into account in the design of multimodal nanoparticles using co-encapsulation strategies.

Introduction

Polymer-based nanoparticles are emerging as promising next generation nano-carriers for therapeutic drug delivery and diagnostic purposes. Tracking the biodistribution of nanoparticles at a cellular level and within the body has, therefore, become an important element of scientific and clinical studies. Thus, the development of nanoparticles capable of supporting multiple imaging platforms to enable tracking at the nanoscale, microscale and whole-animal scale has sparked interest among researchers within the field. Many studies have incorporated superparamagnetic iron oxide nanoparticles within their designs to enable magnetically guided targeting as well as imaging by tissue contrast enhancement in T2-weighted MRI scans[1]. Incorporation of fluorescent dyes allows for imaging at a cellular and histological level by fluorescence microscopy[1,2].

1 School of Chemistry and Biochemistry, The University of Western Australia, 35 Stirling Highway, Crawley 6009, Australia.

2 Experimental and Regenerative Neurosciences, School of Animal Biology, The University of Western Australia, 35 Stirling Highway, Crawley 6009, Australia.

3 Optical+Biomedical Engineering Laboratory, School of Electrical, Electronic and Computer Engineering, The University of Western Australia, 35 Stirling Highway, Crawley 6009, Australia.

4 School of Physics, The University of Western Australia, 35 Stirling Highway, Crawley 6009, Australia.

5 Centre for Microscopy, Characterisation & Analysis, The University of Western Australia, 35 Stirling Highway, Crawley 6009, Australia.

Photon upconversion refers to the sequential absorption of two or more photons which result in an emission of shorter wavelength than the excitation wavelength[3]. The most efficient upconversion materials are fluoride crystals, which have low phonon lattice energies, and are doped with lanthanides such as Yb, Er and Tm[4]. Recent advances in nanoparticle chemistry have allowed for the synthesis of colloidally stable, lanthanide-doped nanoparticles of highly uniform size[5], shape[6] and optical properties[5,7-9]. Upconverting nanomaterials have emerged recently as a new candidate for biological labels[7], due to their inherent photostability and their utilisation of near-infra-red light excitation to probe tissues with greater penetration depths than single-photon fluorescence, whilst overcoming the issues of auto-fluorescence and photo-bleaching that hinder traditional fluorophore probes[8,9]. There have been several reports of using upconverting nanoparticles in combination with iron oxide

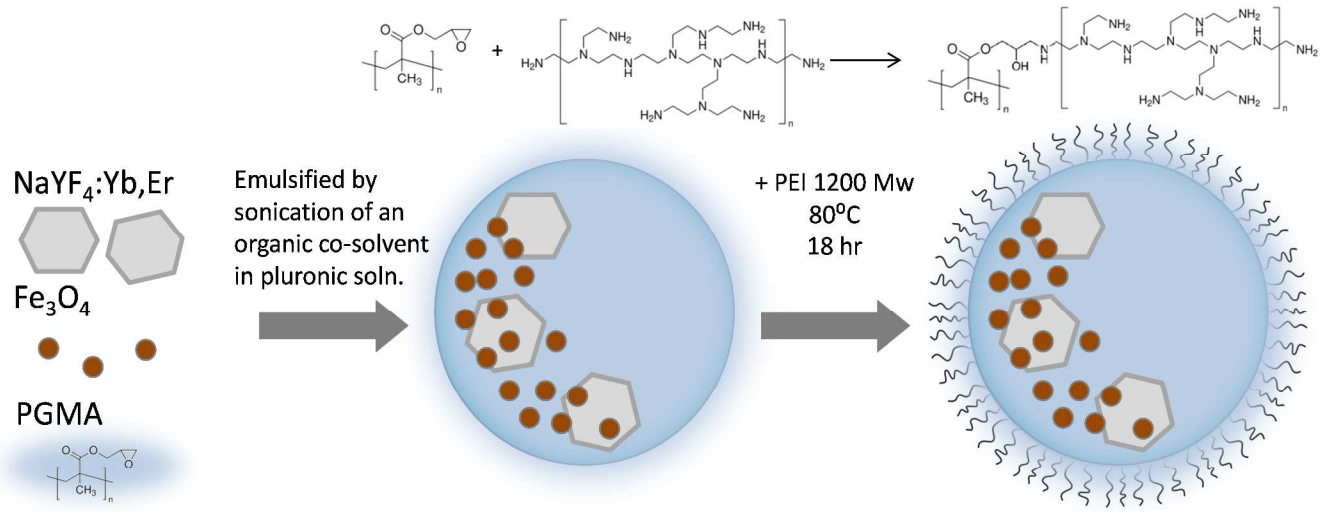

Scheme 1. Using a two-step reaction, upconverting $NaYF_4$:Yb,Er and Fe_3O_4 nanoparticles are co-encapsulated within a PGMA nanosphere. The resulting nanospheres are then coated with the cationic polymer; PEI 1200 Mw, to facilitate cellular uptake.

nanoparticles for biological imaging[10,11]. However, here, we report the importance of the role of upconversion nanoparticle size in designing such constructs. Using poly(glycidyl methacrylate) (PGMA), we co-encapsulate two different sizes of upconverting $NaYF_4$:Yb,Er particles with superparamagnetic iron oxide nanoparticles and coat the construct with polyethylineimine (PEI) to facilitate cellular uptake[12] (Scheme 1). We report the synthesis, characterisation and *in vitro* evaluation of the resultant polymeric nanoparticle system which displays both magnetic and upconversion properties. We demonstrate that the larger upconverting nanoparticles are suitable for biological imaging when used within a single construct with iron oxide nanoparticles, whilst the smaller upconverting particles when used within the same construct are unsuitable due to significant quenching of the emissions.

Results and Discussion

Two batches of polymeric composite nanospheres were synthesised and their optical properties compared. One batch contained 10 nm α-$NaYF_4$:Yb,Er and the other batch 50 nm β-$NaYF_4$:Yb,Er nanoparticles, both co-encapsulated with magnetite nanoparticles (see Materials and Methods section), and the composite nanoparticles produced were found to be colloidally stable by inspection over several weeks, after which visible aggregates formed. However, the particles were easily re-suspended and dynamic light scattering (DLS) measurements confirmed no change in particle size with storage. Size assessment by DLS gave composite nanosphere diameters of ~160 nm and ~220 nm for the 10 nm α-$NaYF_4$:Yb,Er and 50 nm β-$NaYF_4$:Yb,Er polymer particles, respectively (Fig. S2). Before PEI attachment, zeta potentials were -1±4 mV and post PEI attachment, the respective zeta potentials were +23±9 mV and +23±6 mV, which is indicative

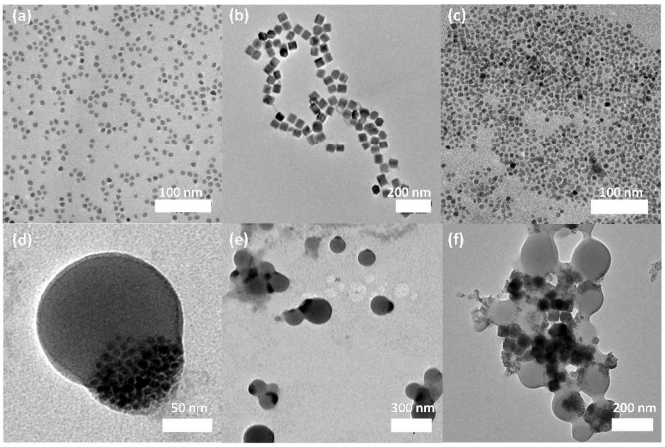

of anchoring of the branched PEI chains to the surface of the nanospheres. Transmission electron microscopy was performed on the magnetite nanoparticles, and on the 10 nm and 50 nm

Figure 1. Transmission electron micrographs of (a) 10 nm α-

$NaYF_4$:Yb,Er (b) 50 nm β-$NaYF_4$:Yb,Er (c) 7 nm Fe_3O_4 particles as synthesised. Polymer composite particles containing Fe_3O_4 with 10 nm α-$NaYF_4$:Yb,Er (d,e) and Fe_3O_4 with 50 nm β-$NaYF_4$:Yb,Er (f) as synthesised.

upconverting nanoparticles to accurately assess their size (Fig. 1 a,b,c, Fig. S1). Select area electron diffraction studies show that the 10 nm $NaYF_4$:Yb,Er nanoparticles are cubic phase (α-$NaYF_4$), whilst the larger, 50 nm $NaYF_4$:Yb,Er nanoparticles conform to the hexagonal phase (β-$NaYF_4$) (Fig. S3, Tables S1, S2).Images taken of the polymer spheres show successful co-encapsulation of Fe_3O_4 and α-$NaYF_4$:Yb,Er (Fig. 1 d,e,). Although it is difficult to distinguish the 10 nm $NaYF_4$:Yb,Er nanoparticles from 7 nm Fe_3O_4 nanoparticles, the 50 nm β-$NaYF_4$:Yb,Er can easily be distinguished from the smaller iron oxide nanoparticles (Fig. 1 f).

The change in nanoparticle phase from cubic to hexagonal is a result of the synthesis method utilised. In order to synthesise the larger, 50 nm β-$NaYF_4$:Yb,Er nanoparticles, the 10 nm, α-$NaYF_4$:Yb,Er initially produced were utilised as seeding particles and were heated once again to elevated temperatures in the presence of $Na(CH_3COO)$ precursor, oleic acid, oleylamine and 1-octadecene (see Materials and Methods for further details of synthesis). Utilising this chemical technique produced significantly larger particles; however, the phase transition was an inevitable consequence of the process. As a result, the two upconverting particles that were utilised for this study were of both a different size and crystal structure. Whilst nanoparticle size and phase were not independently

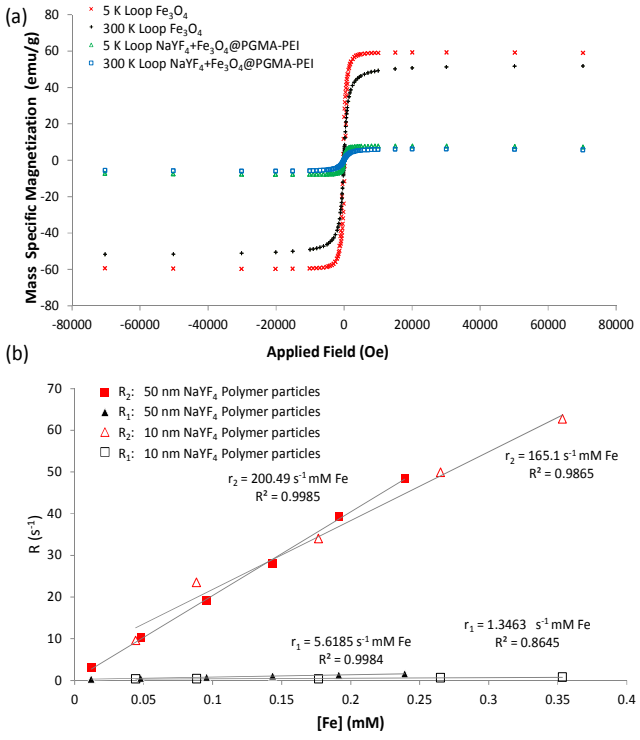

Figure 2. a) Magnetic hysteresis loops acquired at 5 K and 300 K for both magnetite nanoparticles, and 10 nm $NaYF_4$:Yb,Er +Fe_3O_4@PGMA-PEI nanoparticles. (b) Transverse (R_2) and longitudinal (R_1) relaxation rates were measured for varying concentrations of both the 10 nm $NaYF_4$:Yb,Er and 50 nm $NaYF_4$:Yb,Er composite nanospheres to determine the proton relaxivities r_1 and r_2.

varied and tested, for the purposes of this study, these two different forms of the same $NaYF_4$:Yb,Er nanomaterial were investigated as candidates for use in the final magnetic upconversion polymeric composite.

Magnetic and Optical Properties of Nanoparticles

SQUID magnetometry measurements were performed on both the iron oxide nanoparticles and the polymer nanospheres. The 300K hysteresis loops lack any appreciable magnetic hysteresis, which is indicative of superparamagnetic behaviour at this temperature. A rescaled view of the 5K and 300 K hysteresis loops (Fig. S4) of both the iron oxide nanoparticles and the polymer nanospheres suggests that there was no significant change in the magnetic properties during the polymeric encapsulation process, aside from a slight decrease in the high field suceptibility. This is due to the higher relative concentration of diamagnetic components (i.e, the polymer, upconverting particles) in the polymer nanospheres. These results indicate that the magnetite nanoparticles retain their superparamagnetic behaviour in the polymeric composites. The iron oxide nanoparticles make up approximately 12% by mass of the polymer spheres, as calculated from the ratios of the saturation mass-specific magnetizations of the magnetite nanoparticles and the composite polymer spheres.

The suitability of both the 10 nm $NaYF_4$+Fe_3O_4@PGMA-PEI and the 50 nm $NaYF_4$+Fe_3O_4@PGMA-PEI batches of polymer nanoparticles as MRI contrast agents was evaluated by performing concentration series measurements of longitudinal (R_1) and transverse (R_2) proton relaxation rates using a proton relaxometer with a magnetic field strength of 1.4 T. Inductively coupled plasma atomic emission spectroscopy measurements were performed on the most concentrated of the nanoparticle solutions in order to determine the concentration of iron in the samples. Polymer spheres containing magnetite and 10 nm $NaYF_4$:Yb,Er recorded longitudinal and transverse relaxivities of $r_1 = 1.4 \pm 0.3$ mMs^{-1} and $r_2 = 165 \pm 11$ mMs^{-1}, respectively, whilst the polymer spheres containing magnetite and 50 nm $NaYF_4$:Yb,Er recorded $r_1 = 5.6 \pm 0.1$ mMs^{-1} and $r_2 = 200 \pm 4$ mMs^{-1} (Fig 2). The proton transverse relaxivities indicate that both nanospheres are capable of producing significant MRI contrast enhancement in a T_2-weighted scan.

Measurements of upconversion fluorescence were performed on dried solid samples of $NaYF_4$:Yb,Er nanoparticles and polymer composite nanospheres. All measurements were performed under 980 nm excitation (laser intensity of 2850 W/mm^2 for Fig. 3a, b), whilst laser power-dependent measurements were performed under varying laser intensities (1890 W/mm^2 to 8630 W/mm^2) on the $NaYF_4$:Yb,Er particles alone (Fig. 3c, d). It was revealed that for samples of equal mass, the 10 nm α-$NaYF_4$:Yb,Er sample produced observedly less upconversion, compared to the 50 nm β-

$NaYF_4$:Yb,Er sample, which showed ~6.5-fold greater emission intensity (Fig. 3a). This finding is consistent with literature reports which state that, owing to the more favourable

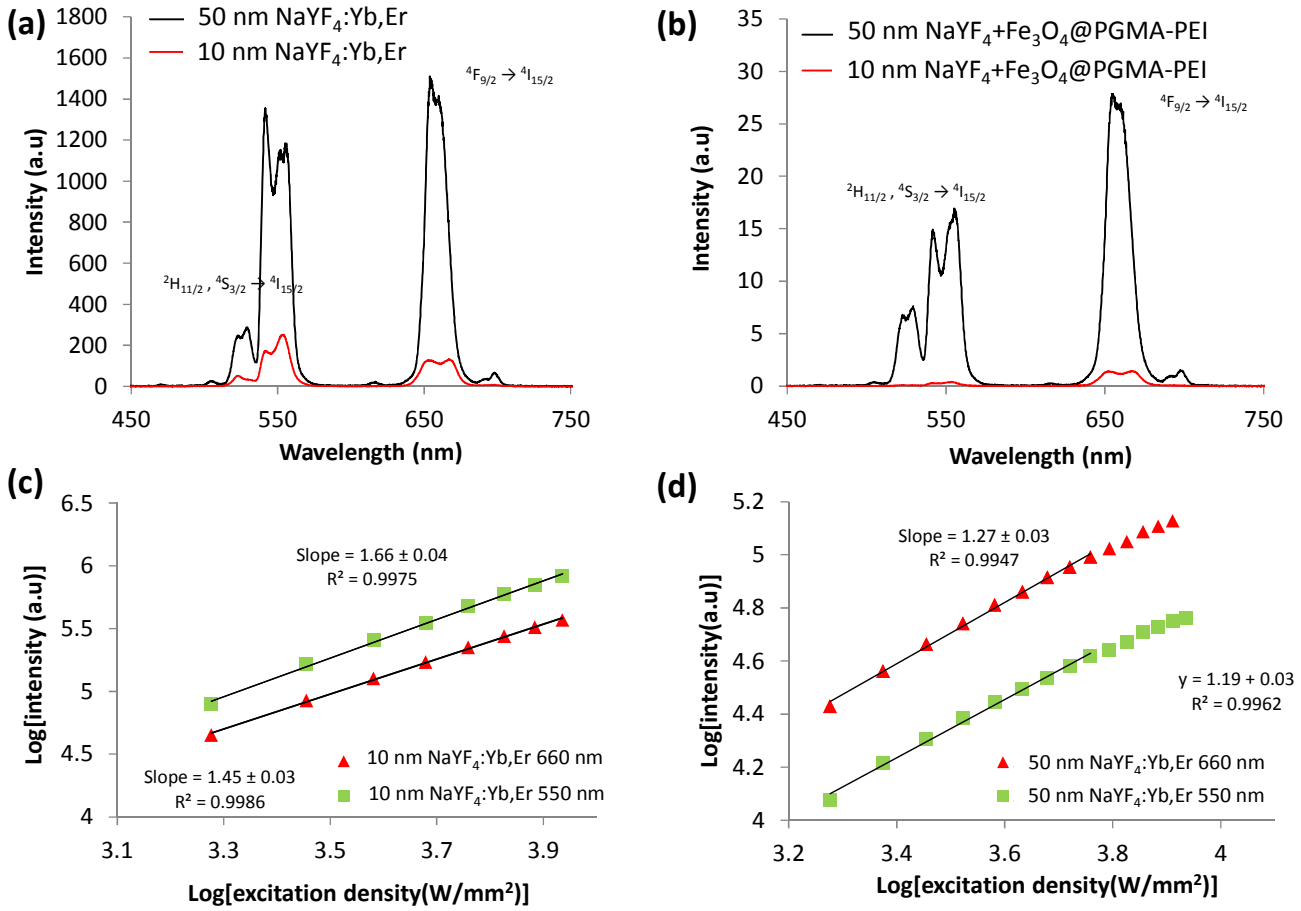

Figure 3. Upconversion spectra recorded for (a) $NaYF_4$:Yb,Er nanoparticles and (b) $NaYF_4$:Yb,Er+Fe_3O_4@PGMA-PEI nanospheres. Log-log plots of emission intensity vs. laser power for both 10 nm (c) and 50 nm (d) particles which illustrate laser power-dependent emissions of nanoparticles.

crystal structure of the hexagonal phase β-$NaYF_4$:Yb,Er, energy transfer upconversion processes may occur more efficiently than in the cubic α-$NaYF_4$:Yb,Er phase, as the lower symmetry of the hexagonal host lattices imparts more uneven crystal-field components to the dopant ions, which increases f-f transition probabilities[13]. Additionally to this, the increased size of the nanoparticles provides a lower surface to volume ratio, which reduces non-radiative transitions to surface ligands in the 50 nm β-$NaYF_4$:Yb,Er as compared to the 10 nm α-$NaYF_4$:Yb,Er. The differences in upconversion efficiencies were further examined by analysing the laser power-dependent emissions of both the 10 nm and 50 nm particles. Both particles show a 1-2 photon dependence on emissions as illustrated in the log-log plots (Fig. 3c,d); however, the slopes were greater for the 10 nm upconversion particles, which show power law exponents of 1.45 ± 0.03 and 1.66 ± 0.04 for red and green emissions; whereas, the 50 nm upconversion particles show exponents of only 1.27 ± 0.03 and 1.19 ± 0.03, indicating more efficient conversion.

The upconversion emissions were also studied for both polymer composite samples (Fig. 3b). Both the smaller 10-nm nanoparticles and the larger 50 nm nanoparticles produced emissions, indicating successful encapsulation of upconverting nanoparticles, though the emission intensities for the 10 nm particles were approximately 36 times weaker (based on average intensities) than the polymer particles containing 50 nm nanoparticles. The relatively lower intensity of upconversion fluorescence in the 10 nm polymer particles can be attributed to the difference in the phase of the $NaYF_4$ lattice and the optical quenching effects imparted by the presence of iron oxide[14] (Fig. S5), which has strong absorption properties in the UV to visible range[15]. Whilst, ideally, 50 nm β-$NaYF_4$:Yb,Er nanoparticles should be compared with smaller β-$NaYF_4$:Yb,Er, 10 nm in size, instead of the 10 nm α-$NaYF_4$:Yb,Er studied herein, increased surface effects arising from sub-20 nm $NaYF_4$:Yb,Er particles[18] significantly decrease upconversion efficiency and therefore, use of any 10 nm $NaYF_4$:Yb,Er nanoparticles would likely lead to significant iron oxide quenching effects when compared with 50 nm size particles.

It was observed that in the polymer spheres, the green $^2H_{11/2}$, $^4S_{3/2} \rightarrow {}^4I_{15/2}$ emissions were more significantly quenched than the red $^4F_{9/2} \rightarrow {}^4I_{15/2}$ (Fig. 3b) in both the 50 nm particles and the 10 nm particles. This is due to the shape of the absorption spectrum of iron oxide, which has a broad absorption band with the highest absorption in the UV-blue region and a gradual decrease until the NIR-region (Fig. S5). This quenching effect makes emissions of 10 nm α-$NaYF_4$:Yb,Er nanoparticles undesirable for biological imaging purposes. The 50 nm β-$NaYF_4$+Fe_3O_4@PGMA-PEI particles proved to still be sufficiently bright to allow for detection by confocal microscopy.

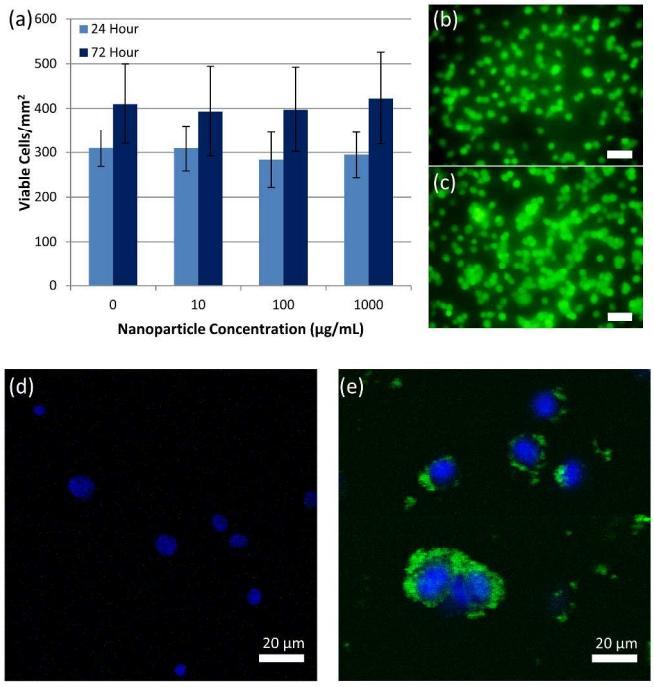

Figure 4 (a) Mean (+/- standard error) live cell viability measurements indicate cells are viable even after exposure to nanoparticles at 1000 µg/mL for 24 or 72 hours (note: different seeding densities for the different times of assessment). Representative images of nanoparticle-exposed cells stained with calcein-AM (green, live cells) and ethidium homodimer (red, dead cells) are provided in (b) and (c) respectively (scale bar: 100 µm). Confocal microscopy shows no visible (green) detection of the 10 nm $NaYF_4$+Fe_3O_4@PGMA-PEI (d), however, the 50 nm $NaYF_4$+Fe_3O_4@PGMA-PEI nanoparticles (green) (e) are clearly visible and show peri-nuclear cytoplasmic localisation (blue, nuclear stain).

Cell Viability and Localisation

Cell viability was measured by incubating PC-12 neural rat cells with varying concentrations of nanoparticle solutions in growth media (from 10 to 1000 µg/mL) for periods of 24 and 72 hours (Fig. 4a). At both the 24 hour and 72 hour time points, there were no statistically significant ($P>0.05$) differences in the number of live cells relative to the controls, even when exposing cells to nanoparticle concentrations as high as 1000 µg/mL (Fig. 4b,c). There were very few dead cells (red) detected in the assays across every treatment group, and as a result, only the live cell count was quantified. The cells appeared to have continued normal growth, and we, therefore, conclude that the nanoparticles do not produce any acute toxic effects on this cell line. Confocal microscopy was performed after incubating PC-12 cells with polymer nanospheres (500 µg/mL) for 24 hours. Cells were cultured on glass coverslips (0.17 mm thickness), fixed for 15 minutes in paraformaldehyde, washed several times with phosphate-buffered saline (PBS) and stained for 15 minutes with a solution of Hoechst 33342 in PBS (0.01 mg/mL) in order to visualise cell nuclei. The coverslips were mounted onto slides using Fluoromount gold mounting media. Imaging of the cells was performed with an inverted Leica TCS SP2 multiphoton confocal microscope. The upconverting components of the nanoparticles were imaged using continuous-wave excitation at a wavelength of 975 nm to track the location of the polymeric nanoparticles. The Hoechst-stained cells were imaged using two-photon excitation at a center wavelength of 800 nm. The resulting images were produced by combining the two channels to assess detectability and cellular uptake. It was found that 10 nm α-$NaYF_4$+Fe_3O_4@PGMA-PEI nanoparticles were undetectable either inside or outside cell nuclei, most likely indicating that this particle formulation is insufficiently bright for confocal imaging. However, the 50 nm β-$NaYF_4$+Fe_3O_4@PGMA-PEI nanoparticles were readily detected and appear to be localised within the cytoplasm but not the nuclei, indicating successful uptake of upconversion nanoparticles by cells (Fig. 4e)[1, 12]. These results suggest that 50 nm β-$NaYF_4$+Fe_3O_4@PGMA-PEI nanoparticles are suitable for tracking by both NIR upconversion fluorescence microscopy and MRI, whilst the upconversion signal of 10 nm $NaYF_4$+Fe_3O_4@PGMA-PEI composites is too greatly quenched to detect under these conditions.

Conclusions:

In conclusion, we have demonstrated the synthesis, characterisation, magnetic properties and *in vitro* evaluation of multifunctional upconverting fluorescent magnetic polymer particles. Our analyses indicate that the size and phase of the upconverting nanoparticles are important considerations that should be taken into account in the design of multimodal polymeric carriers for biological imaging. We showed that both 10 nm and 50 nm sized $NaYF_4$:Yb,Er can be co-encapsulated with magnetite nanoparticles within a PGMA nanosphere to create particles which may be imaged using multiple modalities. Our studies show that 10 nm α-$NaYF_4$:Yb,Er nanoparticles are not suitable when encapsulated in the presence of emission quenching magnetite nanoparticles, but 50 nm β-$NaYF_4$:Yb,Er particles are still capable, even in the presence of magnetite nanoparticles, of producing emissions which can be tracked by confocal microscopy. Both batches of composite nanoparticles show comparable proton transverse

relaxivities, suggesting that the magnetite encapsulated within both particle systems are capable of producing MRI contrast.

Materials and Methods:

Materials:

1200 Mw PEI (50% w/H2O), $Na(CF_3COO)$, $Y(CF_3COO)_3$, $Fe(acac)_3.3H_2O$, 1-Octadecene, oleic acid and oleylamine were purchased from Sigma-Aldrich. Rare-earth precursors $Yb(CF_3COO)_3$ and $Er(CF_3COO)_3$ were purchased from GFS Chemicals.

Iron oxide Nanoparticles

Iron oxide nanoparticles were synthesised using the method described by Sun et al.[19]. 1 mmol of $Fe(acac)_3$ precursor was mixed with 5 mmol of Tetradecanediol, 3 mmol of oleic acid, 3 mmol of oleylamine and mixed in 20 mL of dibenzyl ether. The mixture was heated under an inert atmosphere of nitrogen and magnetically stirred at 100ºC for 1 hour, following which it was heated to 200ºC for 2 hours and finally refluxed at an approximate temperature of 300ºC whilst stirring throughout. The product was allowed to cool and washed with ethanol to yield oleate-capped magnetite nanoparticles of 7 nm in size.

Upconverting Nanoparticles

Upconverting $NaYF_4$:Yb,Er nanoparticles were synthesised using the method of Boyer et al.[16]. 2 mmol of sodium trifluoroacetate, 1.56 mmol of yttrium trifluoroacetate, 0.4 mmol of ytterbium trifluoroacetate, 0.04 mmol of erbium trifluoroacetate, 10 mmol of oleic acid and 10 mmol of oleylamine were mixed in 20 mmol of 1-octadecene. The organic mixture was degassed at 100°C for 30 minutes and rapidly heated to 300°C under N_2 gas. The product was washed with ethanol and yielded a white solid pellet of 10 nm $NaYF_4$ nanoparticles. Larger, 50 nm β-$NaYF_4$:Yb,Er nanoparticles were synthesised by a taking 1 mmol of product from the initial reaction and rapidly heating to 330° C in the presence of 1.3 mmol of sodium trifluoroacetate, 10 mmol of oleic acid and 10 mmol of oleylamine dissolved in 20 mmol of 1-octadecene.

Polymer Nanosphere Preparation

Polyglycidal methacrylate was synthesised by radical polymerization according to the method of Tsyalkovsky et al.[20] In brief, glycidyl methacrylate was polymerized in ethyl methyl ketone (MEK) to give PGMA (Mw= 150,539 g mol), using azobisisobutyronitrile as an initiator. The polymer was purified by multiple precipitations from MEK solution using diethyl ether. Polymer nanospheres were synthesised using a non-spontaneous microemulsion method. 20 mg of Fe_3O_4 nanoparticles, 20 mg of $NaYF_4$:Yb,Er (either the small 10 nm nanoparticles or the large 50 nm particles) and 100 mg of poly(glycidal methacrylate) were dissolved in a co-solvent of chloroform and ethyl methyl ketone (3 mL and 9 mL). The organic phase was added dropwise to a 1.25% w/w surfactant solution of Pluronic (F-108) under heavy stirring and then sonicated for one minute. The solution was left to stir under heavy nitrogen flow for a period of 1 hour so that all chloroform and MEK were evaporated. Following this step, 100 mg of 50% w/w PEI 1200 Mw was mixed in and stirred overnight at a temperature of 80^0C to allow reaction of the primary amine groups of PEI with the glycidyl rings on the PGMA nanospheres. The nanoparticles were then centrifuged at 3000 RPM for 40 minutes to remove large unsuspended aggregates of PGMA, magnetite and $NaYF_4$:Yb,Er. The nanoparticles were then collected and washed using a magnetic separation column. This step ensured that the non-magnetic fraction of the particle solution was removed, such that all particles collected contained magnetite.

Upconverting Nanoparticle Analysis

Upconverting nanoparticles were analysed by drying solutions (100 μg/μL) of nanoparticles onto glass slides and measuring their upconversion spectra using a custom optical setup (Fig. S6). Approximately 700 μg of nanoparticles were added to each slide. The 975 nm excitation light from a laser diode was focused onto the nanoparticles using an objective lens with a numerical aperture (NA) of 0.4. The emitted upconversion fluorescence was collected using the same objective lens and directed to a spectrometer via a dichroic beamsplitter (edge wavelength 900 nm) and a band-pass filter for blocking any returning excitation light (transmission range: 315 – 710 nm). The peak wavelength of the laser diode is 974.5 nm. The excitation power was adjusted by altering the forward bias current supplied to the laser diode (20-100 mA) and the temperature of the laser diode was held at a constant value of 25°C via the integrated thermoelectric cooler.

Cell Culture

Neuronal PC-12 cells were cultured in RPMI media with 10% horse serum, 5% fetal bovine serum (FBS), 1% L-glutamine, 1% penicillin/streptomycin, 1% non-essential amino acids and 1% sodium pyruvate (Invitrogen). All well plates were coated with a 1% poly-ι-lysine solution for one hour, and rinsed thoroughly with PBS before plating. Cells were seeded at densities of $2x10^5$ cells/mL for the 24 hour assay, and $1x10^5$ cells/mL for the 72 hour assay. The following day, media was removed and replaced with UV-sterilised media containing nanospheres at concentrations of 0 μg/mL, 10 μg/mL, 100 μg/mL and 1000 μg/mL (5 replicates). The toxicity of the synthesised nanoparticles was assessed by use of a live-dead fluorescence assay, utilising 1μM calcein-AM (green, live cells) and 2μM ethidium homodimer (red, dead cells) dissolved in PBS to stain the cells (Invitrogen). Viability was quantified by counting all viable cells in four fields of view per well. Fields of view were randomly assigned and consistent for all culture wells. An Olympus IX51 inverted fluorescence microscope was used for cell viability assessments. For statistical analyses on cell counts for all nanoparticle concentrations, one-way analysis of variance (ANOVA) tests and a Bonferroni post-hoc test for comparison of means were performed to determine statistically

significant concentration-dependent effects of nanoparticles on cellular viability.

Confocal Microscopy of Upconverting Nanoparticles

Samples for confocal microscopy were prepared by seeding cells onto glass cover slips, and exposing the cells to 500 µg/mL nanoparticle solutions of 10 nm $NaYF_4$:Yb,Er +Fe_3O_4@PGMA-PEI in media and 50 nm $NaYF_4$:Yb,Er +Fe_3O_4@PGMA-PEI in media. After 24 hours, cells were fixed with paraformaldehyde, stained with Hoechst 33342 (Invitrogen) and mounted onto glass slides for confocal imaging. Confocal microscopy was performed using an inverted Leica TCS SP2 confocal microscope. The excitation source was a wavelength-tuneable Ti:Sapphire laser which can be operated both in pulsed and in continuous-wave mode (Mai-Tai, Spectra-Physics, tuning range 710-990nm). For imaging of the Hoechst stain, the laser was operated in pulsed mode at a center wavelength of 800 nm with the detection window 400 – 450 nm. For tracking upconversion nanoparticles, the laser was operated in continuous-wave mode at 975 nm with the detection window 515 – 675 nm. Imaging was performed using a Leica HCX PL APO 40x, 1.25 NA oil immersion objective lens.

Proton Relaxometry and SQUID Magnetometry Measurements

Magnetic properties of the particles were measured using a Quantum Design MPMS® (Magnetic Property Measurement System) SQUID magnetometer. The sample is cooled using a flow of liquid helium which allows its magnetic properties to be determined between temperatures of 5 K and 300 K in fields of up to 7 T. Hysteresis loop scans were performed on samples at 5K and 300K, to characterize and confirm the superparamagnetic nature of the particles at ambient temperature. Proton relaxometry measurements were performed on dilute suspensions of nanoparticles, using a Bruker minispec mq60 relaxometer, with a frequency of 60 MHz and a field strength of 1.4 T. A dilution series of nanoparticle solutions in water were measured for each composite particle formulation to assess concentration-dependent relaxation rates of the suspensions.

Acknowledgements

The authors acknowledge the facilities and the scientific and technical assistance of the Australian Microscopy & Microanalysis Research Facility at the Centre for Microscopy, Characterisation & Analysis, The University of Western Australia, a facility funded by the University, State and Commonwealth Governments.

Corresponding Author: * swaminatha.iyer@uwa.edu.au

Author Contributions

The manuscript was written through contributions of all authors. All authors have given approval to the final version of the manuscript.

Funding Sources

Michael Challenor acknowledges the Graduate Research School of The University of Western Australia for funding in the form of an Australian Postgraduate Award Scholarship. Peijun Gong is supported by The University of Western Australia and the China Scholarship Council. The authors acknowledge funding from the Australian Research Council and the National Health and Medical Research Council.

References

1. Evans, C. W.; Latter, M. J.; Ho, D.; Peerzade, S. A. M. A.; Clemons, T. D.; Fitzgerald, M.; Dunlop, S. A.; Iyer, K. S., Multimodal and multifunctional stealth polymer nanospheres for sustained drug delivery. *New J. Chem.* **2012,** *36* (7), 1457-1462.
2. Na, H. B.; Song, I. C.; Hyeon, T., Inorganic nanoparticles for MRI contrast agents. *Adv. Mater.* **2009,** *21* (21), 2133-2148.
3. Haase, M.; Schäfer, H., Upconverting nanoparticles. *Angew. Chem. (International ed. in English)* **2011,** *50* (26), 5808-5829.
4. Auzel, F., Upconversion and anti-Stokes processes with f and d ions in solids. *Chem. Rev.-Columbus* **2004,** *104* (1), 139-174.
5. Wang, F.; Han, Y.; Lim, C. S.; Lu, Y.; Wang, J.; Xu, J.; Chen, H.; Zhang, C.; Hong, M.; Liu, X., Simultaneous phase and size control of upconversion nanocrystals through lanthanide doping. *Nature* **2010,** *463* (7284), 1061-1065.
6. Ye, X.; Collins, J. E.; Kang, Y.; Chen, J.; Chen, D. T. N.; Yodh, A. G.; Murray, C. B., Morphologically controlled synthesis of colloidal upconversion nanophosphors and their shape-directed self-assembly. *PNAS* **2010,** *107* (52), 22430-22435.
7. Boyer, J.-C.; Vetrone, F.; Cuccia, L.; Capobianco, J., Synthesis of colloidal upconverting $NaYF_4$ nanocrystals doped with Er3+, Yb3+ and Tm3+, Yb3+ via thermal decomposition of lanthanide trifluoroacetate precursors. *J. Am. Chem. Soc.* **2006,** *128* (23), 7444-7445.
8. Chatterjee, D. K.; Gnanasammandhan, M. K.; Zhang, Y., Small upconverting fluorescent nanoparticles for biomedical applications. *Small* **2010,** *6* (24), 2781-2795.
9. (a) Wang, F.; Liu, X., Upconversion multicolor fine-tuning: visible to near-infrared emission from lanthanide-doped $NaYF_4$ nanoparticles. *J. Am. Chem. Soc.* **2008,** *130* (17), 5642-5643; (b) Wang, F.; Liu, X., Recent advances in the chemistry of lanthanide-doped upconversion nanocrystals. *Chem. Soc. Rev.* **2009,** *38* (4), 976-989.
10. Liu, Y.; Tu, D.; Zhu, H.; Chen, X., Lanthanide-doped luminescent nanoprobes: controlled synthesis, optical spectroscopy, and bioapplications. *Chem. Soc. Rev.* **2013,** *42* (16), 6924-6958.
11. Wang, F.; Banerjee, D.; Liu, Y.; Chen, X.; Liu, X., Upconversion nanoparticles in biological labeling, imaging, and therapy. *The Analyst* **2010,** *135* (8).

12. Shili, G.; Piaoping, Y.; Chunxia, L.; Wenxin, W.; Yunlu, D.; Na, N.; Jun, L., Synthesis of magnetic, up-conversion luminescent, and mesoporous core-shell-structured nanocomposites as drug carriers. *Adv. Funct. Mater.* **2010,** *20*.
13. Liang, C.; Chao, W.; Xinxing, M.; Qinglong, W.; Yao, C.; Han, W.; Yonggang, L.; Zhuang, L., Multifunctional upconversion nanoparticles for dual-modal imaging-guided stem cell therapy under remote magnetic control. *Adv. Funct. Mater.* **2013,** *23* (3), 272-280.
14. Evans, C. W.; Fitzgerald, M.; Clemons, T. D.; House, M. J.; Padman, B. S.; Shaw, J. A.; Saunders, M.; Harvey, A. R.; Zdyrko, B.; Luzinov, I.; Silva, G. A.; Dunlop, S. A.; Iyer, K. S., Multimodal analysis of PEI-mediated endocytosis of nanoparticles in neural cells. *ACS nano* **2011,** *5* (11), 8640-8648.
15. Yi, G. S.; Chow, G. M., Synthesis of hexagonal-Phase $NaYF_4$:Yb,Er and $NaYF_4$:Yb,Tm nanocrystals with efficient up-conversion fluorescence. *Adv. Funct. Mater.* **2006,** *16* (18), 2324-2329.
16. Challenor, M.; Gong, P.; Lorenser, D.; Fitzgerald, M.; Dunlop, S.; Sampson, D. D.; Swaminathan Iyer, K., Iron Oxide-Induced Thermal Effects on Solid-State Upconversion Emissions in NaYF4:Yb,Er Nanocrystals. ACS Appl. Mater. Interfaces 2013, 5 (16), 7875-7880.
17. He, Y. P.; Miao, Y. M.; Li, C. R.; Wang, S. Q.; Cao, L.; Xie, S. S.; Yang, G. Z.; Zou, B. S.; Burda, C., Size and structure effect on optical transitions of iron oxide nanocrystals. *Phys. Rev. B* **2005,** *71* (12), 125411.
18. D. J. Gargas, E. M. Chan, A. D. Ostrowski, S. Aloni, M. V. P. Altoe, E. S. Barnard, B. Sanii, J. J. Urban, D. J. Milliron, B. E. Cohen, and P. J. Schuck, Engineering bright sub-10-nm upconverting nanocrystals for single-molecule imaging, *Nat. Nanotechnol.*, vol. 9, no. 4, pp. 300–305, Apr. 2014.
19. Sun, S.; Zeng, H.; Robinson, D.; Raoux, S.; Rice, P.; Wang, S.; Li, G., Monodisperse MFe2O4 (M = Fe, Co, Mn) nanoparticles. *J. Am. Chem. Soc.* **2004,** *126* (1), 273-279.
20. Tsyalkovsky, V.; Klep, V.; Ramaratnam, K.; Lupitskyy, R.; Minko, S.; Luzinov, I., Fluorescent reactive core–shell composite nanoparticles with a high surface concentration of epoxy functionalities. *Chem. Mater.* **2008,** *20* (1), 317-325.

TOC Graphic:

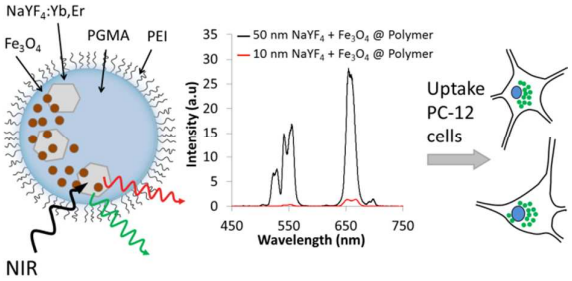

Table of contents sentence:

Polymeric composites incorporating upconversion nanoparticles and superparamagnetic iron oxide nanoparticles were synthesised and assessed as multimodal imaging probes *in vitro*.

Keywords:

Upconversion, Magnetite, Quenching, Nanoparticles, Sensing